Наносистеми, наноматеріали, нанотехнології
Nanosistemi, Nanomateriali, Nanotehnologii
2026, т. 24, № 1, сс. 83–96
https://doi.org/10.15407/nnn.24.01.0083

PACS numbers: 07.05.Tp, 42.70.Qs, 73.30.+y, 78.40.Ha, 78.67.-n, 84.60.Jt, 88.40.hj

Improving the Efficiency of Lead-Free Nanoperovskite Cells Using SCAPS-1*D* Software

Hardan T. Ghanem[1], Muaamar A. Kamil[2], and Mahmood H. Mayoof[3]

[1]*Shirqat Department,*
Salah al-Din Education Directorate, Ministry of Education,
34001 Shirqat, Iraq
[2]*College of Education for Pure Sciences,*
Department of Physics,
Tikrit University,
34001 Tikrit, Iraq
[3]*Anbar Education Directorate, Ministry of Education,*
34001 Anbar, Iraq

The OMeATP/$Cs_2AgBiBr_6$/TiO_2/FTO solar cell is studied using SCAPS-1*D* simulation, where a compound with nanoparticles with sizes ranging from 1.2 to 2.9 nm is used. Previous practical research is compared with the program, and good results are obtained that mimic the results of the practical research used. The cell is improved by increasing the work function; so, the conversion efficiency is increased from 0.31% to 1.01%. The distortion rate of the reflection layer is increased; so, the efficiency is increased from 1.01% to 1.22%. The thickness of the absorption layer is changed; so, the efficiency is increased from 1.22% to 3.91%. Then, the radiation recombination coefficient is changed. It is noticed that the cell efficiency is increased and the recombination is decreased; so, the efficiency is increased from 3.91% to 4.79%.

Сонячний елемент OMeATP/$Cs_2AgBiBr_6$/TiO_2/FTO досліджено за допомогою моделювання симулятором ємности сонячних елементів SCAPS-1*D*, де використано сполуку з наночастинками розміром від 1,2 до 2,9 нм. Попередні практичні дослідження порівняно з програмою й одержано хороші результати, що імітують результати використаних практичних досліджень. Елемент вдосконалено шляхом збільшення роботи виходу; тому ефективність перетворення збільшилася від 0,31% до 1,01%. Швидкість спотворення шару відбивання збільшено; тому ефективність збільшилася від 1,01% до 1,22%. Товщину шару вбирання змінено; тому ефективність збільшилася від 1,22% до 3,91%. Потім змінено коефіцієнт рекомбінації випромінення. Помічено, що ефективність елементу збільшилася, а рекомбінація зменшилася; тому ефективність збільшилася від 3,91% до 4,79%.

Key words: nanoperovskite, $Cs_2AgBiBr_6$, SCAPS simulation, absorption layer, distortion rate, efficiency.

Ключові слова: наноперовськіт, $Cs_2AgBiBr_6$, СЄСЕ-моделювання, вбиральний шар, швидкість спотворення, ефективність.

(Received 18 July, 2024; in revised form, 8 August, 2024)

1. INTRODUCTION

Over the past ten years, lead-halide perovskite (LHP) nanocrystals have garnered a great deal of attention because of their exceptional optical and optoelectronic qualities, which include long photocarrier diffusion lengths, low exciton binding energies, and high photoluminescence quantum yields (PL QYs) [1–3]. Over the past ten years, lead-halide perovskite (LHP) nanocrystals have garnered a great deal of attention because of their exceptional optical and optoelectronic qualities, which include long photocarrier diffusion lengths, low exciton binding energies, and high photoluminescence quantum yields (PL QYs) [4, 5]. The materials exhibit diffusion of both holes and electrons of more than approximately one micron, and the diffusion length means that these materials can operate effectively in a thin structure, and that charges can be transported in the perovskite itself over long distances [6, 7]. Recent research has indicated that the charges of perovskites always exist in the form of free electrons and holes, rather than as bound excitons, because the exciton binding energy is low enough to enable charge separation at room temperature [8]. Double perovskite materials, $Cs_2AgBiBr_6$, have been discovered, as they are layered. Absorption is suitable for the manufacture of solar cells, as it is a highly crystalline compound, which encourages energy generation [9, 10], as it is more stable because it is not affected by moisture [11]. In this research, we will take the main absorption layer, the perovskite compound $Cs_2AgBiBr_6$, which is a double layer that is free of toxicity and less affected by humidity, with a back reflection layer, OMeTAD, a matching layer, TiO_2, and FTO permeation. The theoretical work was compared with experimental work, and a great convergence in the results was revealed, to show the extent of the program sobriety, because we performed an improvement on the cell generated through the SCAPS-1*D* program.

2. NUMERICAL SIMULATION IN SCAPS

Modelling can be performed using the SCAPS program, which is a one-dimensional solar cell simulation program designed at the Uni-

versity of Ghent in Belgium to simulate traditional semiconductor crystalline materials such as CIGS, CdTe, or other materials such as SnS. The user can describe a cell consisting of a maximum of seven layers for different properties such as optical absorption, thickness, doping concentration, energy gap, *etc*. The spectral responses are determined and can be calculated in the dark and in the light as a function of temperature. This program has been developed and applied to all solar cells. It is a program is available free. The program is based on solving semiconductor equations. We begin by writing the Poisson equation, an elliptical partial differential equation, named after the French physicist Simeon Poisson, who discovered its application in universal gravity and static electricity with the equation also known by its name, the Poisson–Boltzmann equation, which regulates the relationship between electric potential and the distribution of electric charge, and in general, it has applications in quantum theory [12, 13]:

$$\nabla E = \frac{q}{\varepsilon}\left(p - n + N_D^+ - N_A^- \right). \tag{1}$$

Then, the continuity equation gives the following relationships [14]:

$$\frac{dn}{dt} = \frac{1}{q}\left(\nabla J_n + G_n - R_n \right), \tag{2}$$

$$\frac{dp}{dt} = -\frac{1}{q}\left(\nabla J_p + G_p - R_p \right). \tag{3}$$

Finally, the charge carrier equations for the diffusion and drift current density can be obtained from the following equations [15]:

$$J_n = q\left(\mu_n nE + D_n \nabla n \right), \tag{4}$$

$$J_p = q\left(\mu_p PE + D_p \nabla p \right). \tag{5}$$

To measure the quality of photovoltaic cells, fill factor (*FF*), short circuit current J_{sc}, open circuit voltage V_{oc}, and conversion efficiency η must be known, as these variables are related to each other with the following equations [15]:

$$FF = \frac{P_{\max}}{P_t} = \frac{V_{\max} I_{\max}}{V_{oc} J_{sc}}, \tag{6}$$

$$\eta = \frac{P_{\max}}{P_{in}} = \frac{V_{oc} J_{sc} FF}{P_{in}}. \tag{7}$$

The age of the minority carriers can be determined, which is the

average time required for the recombination of the minority carriers, and it is linked to the doping concentration and recombination by the following relationships [16]:

$$\eta = (\sigma V_{th} N_t)^{-1}, \tag{8}$$

$$\tau = \Delta n / R. \tag{9}$$

The saturation current equation for the diode is one of the important equations, which determines the effect of propagation length and carrier density on cell performance [12, 15]:

$$I_0 = \left[\frac{q D_n n_i^2}{L_n N_A} + \frac{q D_p n_i^2}{L_p N_D} \right]. \tag{10}$$

Likewise, quantum efficiency (QE) greatly affects the performance of the cell, whose equation can be written [16, 17] as follows:

$$QE = 1.24 R_\lambda / \lambda . \tag{11}$$

3. SOLAR CELL INSTALLATION

The OMeATP/$Cs_2AgBiBr6$/TiO_2/FTO solar cell consists of a FTO window layer of transparent metal oxides that has a relatively large energy gap; then, it is followed by the TiO_2 compatibility layer, which has an energy gap suitable for the gradient of the absorption layer with the penetration, and then the $Cs_2AgBiBr_6$ absorption layer, which has a relatively small energy gap and forget. It has a flat band front and silver ohmic contact with a work function 4.26 V and the cell is on a glass floor [18]. Table 1 gives the values of the program parameters. Table 2 gives the values of the defects that must be entered in the absorption layer for the SCAPS program to study the performance of the experimental cell. The temperature was 300 K. Figure 1 shows the installation of the solar cell.

To enhance the efficiency of solar cells, we must work on: compare the experimental cell with the theoretical cell; optimize the cell by changing the back-connection work function; improve the cell by changing the thickness and the impurity ratio to obtain the best cell.

4. DISCUSSION OF RESULTS

4.1. Comparing the Experimental Cell with the Theory

To simulate the performance of the solar cell, the program used must be verified and the extent of its conformity with the practical

TABLE 1. Physical parameters for all layers [19–23].

Parameters	Symbol, unit	OMeTAD	$Cs_2AgBiBr_6$	TiO_2	FTO
Thickness	W, μm	0.05	0.5	0.07	0.05
Band gap	E_g, eV	2.9	2.05	3.45	3.5
Electron affinity	χ, eV	2.2	4.19	4.2	4
Dielectric permittivity	ε_r	3.0	5.8	10	9
CB effective density of states	N_C, cm^{-3}	$2.5 \cdot 10^{18}$	$1.0 \cdot 10^{16}$	$2.2 \cdot 10^{18}$	$2.2 \cdot 10^{18}$
VB effective density of states	N_V, cm^{-3}	$2.2 \cdot 10^{18}$	$1.0 \cdot 10^{16}$	$1.8 \cdot 10^{19}$	$1.8 \cdot 10^{19}$
Electron thermal velocity	V_n, cm/s	$1.0 \cdot 10^{7}$	$1.0 \cdot 10^{7}$	$1.0 \cdot 10^{7}$	$1.0 \cdot 10^{7}$
Hole thermal velocity	V_P, cm/s	$1.0 \cdot 10^{7}$	$1.0 \cdot 10^{7}$	$1.0 \cdot 10^{7}$	$1.0 \cdot 10^{7}$
Electron mobility	μ_n, $cm^2/(V \cdot s)$	$1 \cdot 10^{-4}$	11.8	100	20
Hole mobility	μ_p, $cm^2/(V \cdot s)$	$1 \cdot 10^{-4}$	6.49	25	10
Shallow uniform donor density	N_D, $1/cm^3$	0	$1.0 \cdot 10^{19}$	$1.0 \cdot 10^{19}$	$1.0 \cdot 10^{20}$
Shallow uniform acceptor density	N_A, $1/cm^3$	$1.0 \cdot 10^{19}$	$1.0 \cdot 10^{19}$	0	0
Coefficient absorption	α, 1/cm	$1.0 \cdot 10^{5}$	$4.5 \cdot 10^{3}$	$1.0 \cdot 10^{5}$	$1.0 \cdot 10^{5}$
Radiative recombination coefficient	cm^3/s	$1.0 \cdot 10^{-9}$	$4.0 \cdot 10^{-9}$	$2.3 \cdot 10^{-9}$	$2.3 \cdot 10^{-9}$

TABLE 2. Surface defects and absorption layer defects.

Characteristics of defects	Surface defects OMeTAD/$Cs_2AgBiBr_6$	Absorption defects *p*-$Cs_2AgBiBr_6$	Surface defects $Cs_2AgBiBr_6/TiO_2$
Energy level with respect to reference, eV	1.3	0.6	1.3
Total density, N_t, cm^{-2}	$1.0 \cdot 10^{7}$	$1.0 \cdot 10^{13}$	$1.0 \cdot 10^{9}$
Capture cross section area of electrons, δ_e, cm^2	$2.3 \cdot 10^{-18}$	$1.0 \cdot 10^{-15}$	$2.3 \cdot 10^{-18}$
Capture cross section area of holes, δ_h, cm^2	$2.3 \cdot 10^{-18}$	$1.0 \cdot 10^{-15}$	$2.3 \cdot 10^{-18}$

results must be verified. We conducted a simulation of the practical research by FAN, Ping *et al.* [24] on the SCAPS program, and the results showed a great match between the practical and theoretical results, as shown in Table 3, but the match is not complete.

Among the results, it is a decrease in the filling factor, which led to a decrease in the conversion efficiency. The reason is due to the defects in the interface P-OMeATD/$Cs_2AgBiBr_6$, *p*-$Cs_2AgBiBr_6/TiO_2$ and the defects in the absorption layer *p*-$Cs_2AgBiBr_6$. With a de-

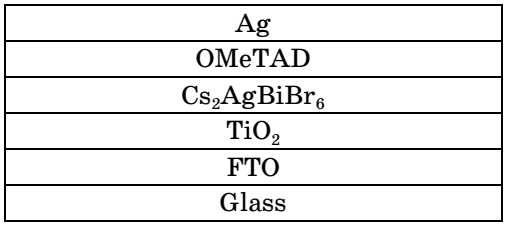

Fig. 1. Solar cell installation.

TABLE 3. Theoretical and experimental cell outputs.

Solar cell	V, V	J, mA/cm^2	FF, %	η, %
OMeATD/$Cs_2AgBiBr_6$/TiO_2/FTO (Experimental) [24]	0.87	1.24	0.65	0.70
OMeATD/$Cs_2AgBiBr_6$/TiO_2/FTO (Theoretical)	0.84	2.61	32.2	0.72

crease in N_t defects, the correspondence of the experimental work with the theory increases, due to the increase in durability. Minority carriers, which are inversely proportional to defects, as shown in Eq. (8); so, recombination will decrease, and as shown in Eq. (9), the efficiency of the theoretical cell increases over the experimental cell.

4.2. Effect of the Work Function

The layers of the solar cell consist of semiconductor materials and have a front connection and a back connection to transfer electrical power outside the cell. The front connection is between a metal and a semiconductor, and its resistance is very small compared to the resistance of the device. It is called ohmic contact because the resistance is very small [25]. Ohmic contact depends on the form Main on the relative difference between the work function of a conductor and the electronic affinity of a semiconductor material. The work function can be defined as the lowest binding energy of an electron to the surface of the metal. The front connection in the program has a flat band icon, but the back connection has a certain resistance and is called as the Schottky connection.

The Schottky connection works the opposite of the ohmic connection, as it does not allow current to flow except in one direction, that is, it resembles a one-sided p–n diode. Therefore, we notice that the concentration of carriers on the conductive side is much higher than its focus is on Semi Mosul. For the back connection, silver metal was used [26], and the work function was changed from

4.2 eV to 4.9 eV. We noticed an increase in the conversion efficiency, fill factor, and open circuit voltage. This is because for a *p*-type metal-semiconductor connection, the work function of the metal is less than the work function of the semiconductor, which leads to the flow of electrons from the conductor to the semiconductor, and increasing the work function helps to achieve quickly a state of thermal equilibrium [27].

Figure 2 shows the effect of the work function on the cell outputs. Figure 3 shows the relationship of voltage with current, and we notice an increase in efficiency and fill factor with an increase in the work function. Quantum efficiency was studied, which is the percentage of the number of carriers generated in the cell to the number of photons falling on the solar cell.

Figure 4 shows the relationship of wavelength as a function of quantum efficiency, and we notice that there is no it as affected by the change in the work function because it depends on the spectral response and wavelength [16, 17].

4.3. Effect of Acceptance on Reflection Layer

The distortion of the back reflection layer was changed from $1 \cdot 10^{19}$ cm^{-3} to $1 \cdot 10^{22}$ cm^{-3} so we noticed an increase in the conversion efficiency and filling factor, and Fig. 5 shows the change.

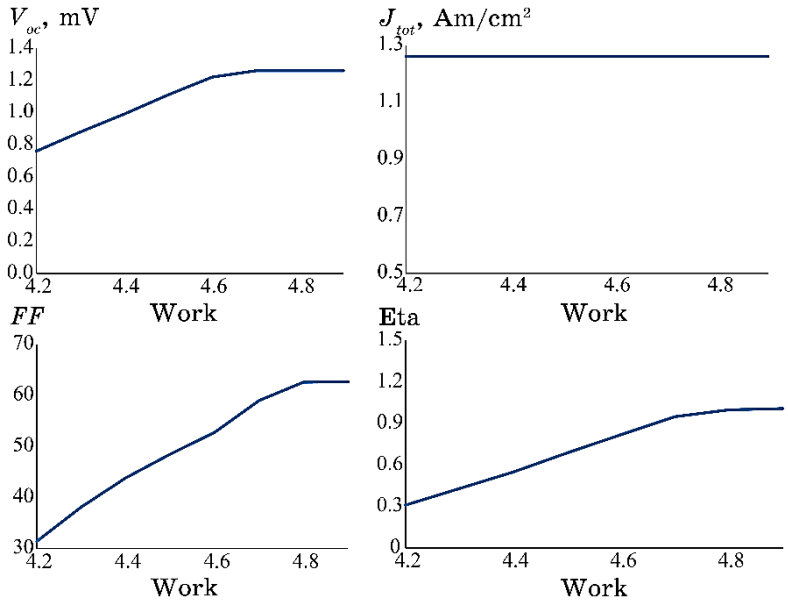

Fig. 2. Work function as a function of cell output.

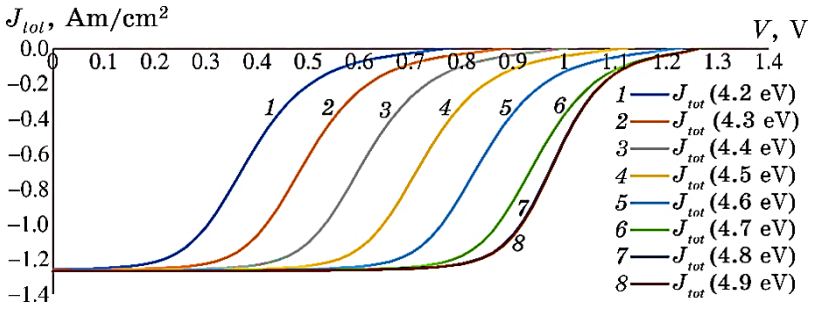

Fig. 3. Voltage as a function of current.

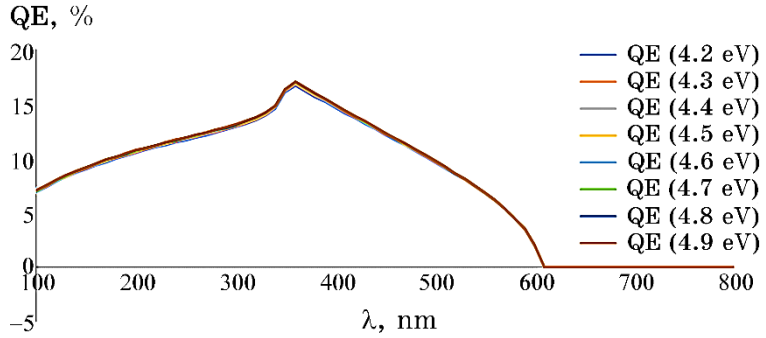

Fig. 4. Wavelength as a function of quantum efficiency.

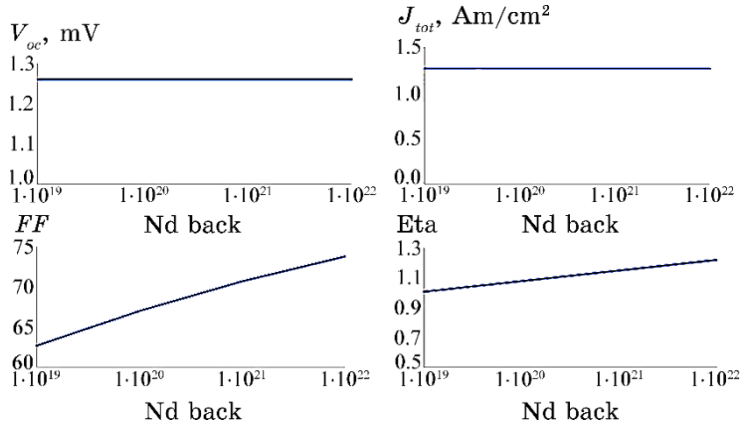

Fig. 5. Percentage of midwife defects as a function of cell output

The cell outputs increase the doping ratio, because increasing the doping ratio leads to an increase in carriers; so, the saturation current of the cell decreases, as shown in Eq. (10). Figure 6 shows the

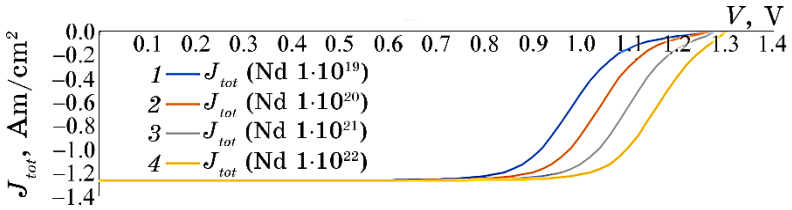

Fig. 6. Voltage as a function of current.

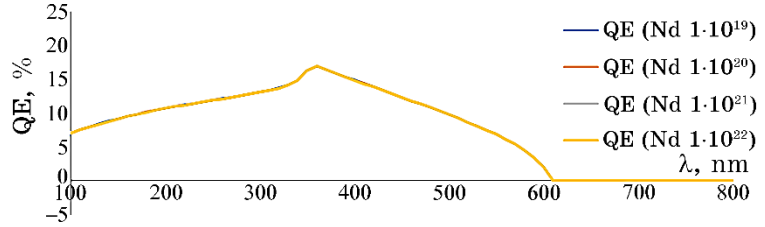

Fig. 7. Relationship of wavelength with quantum efficiency nm.

relationship of voltage with current. Figure 7 shows the relationship of wavelength with quantum efficiency, and that quantum efficiency begins at 7% at the length. The wavelength is of 100 nm and increases to 17% with the greatest amount at the wavelength of 370 nm; then, it begins to decrease gradually until it reaches zero. The reason is that the length of propagation decreases and the absorbance is at the lowest amount at high wavelengths because the efficiency is inversely proportional to the wavelength according to Eq. (11) [28].

4.4. Effect of Thickness and Radiation Recombination of the Absorption Layer

The thickness of the absorption layer was changed from 0.5 μm to 2.5 μm. We noticed an increase in the shunt efficiency and a decrease in the fill factor and short circuit current, as shown in Fig. 8. This is because increasing the thickness leads to an increase in the absorption of photons, so the generation of the electron-gap pair increases and the recombination process at the interface decreases, which leads to an increase in the optical current [29, 30].

Figure 9 shows the relationship of voltage with current.

Figure 10 shows the wavelength with quantum efficiency. Notice the increase in quantum efficiency that starts at the smallest thickness of 7% until it reaches 15% at the largest thickness, where the quantum efficiency increases and reaches the greatest amount of

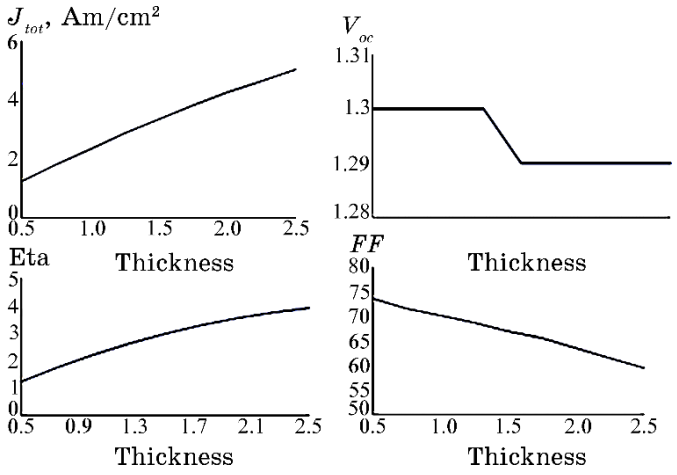

Fig. 8. Thickness as a function of cell output.

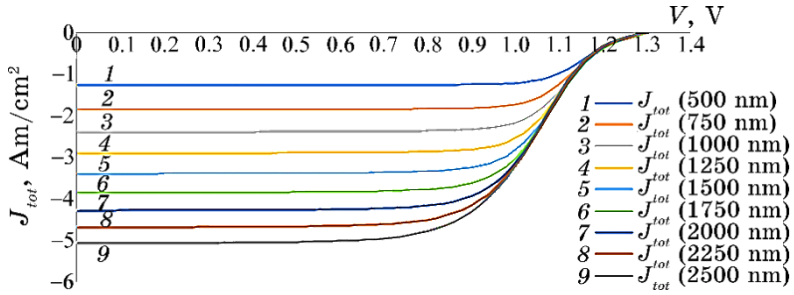

Fig. 9. Voltage as a function of current for different absorption layer thicknesses.

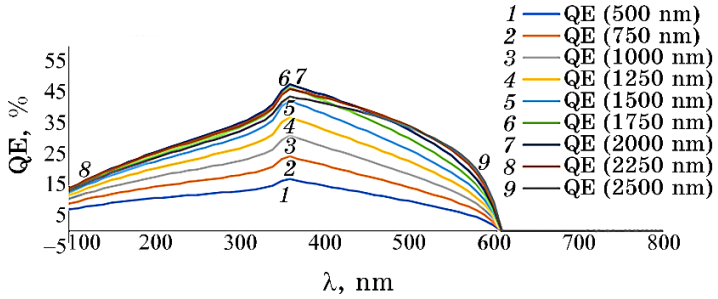

Fig. 10. Wavelength as a function of quantum efficiency for different absorption layer thicknesses.

45% at the wavelength of 370 nm; then, it begins to decrease.

Therefore, because the value of the absorption coefficient is high at short wavelengths, absorption occurs near the surface because the recombination time is short; so, the previously generated carriers are captured by the p–n crystal diode [31].

Figure 11 shows the relationship of recombination with the cell output. You notice an increase in cell efficiency and fill factor whenever recombination decreases, with both current and voltage remaining constant, because the decrease in recombination increases the durability of the minority carriers, which increases the cell efficiency according to Eq. (8) and Eq. (9), due to the increase in the voltage barrier [32, 33].

Figure 12 shows the relationship of voltage with current. Figure 13 shows the relationship of wavelength with quantum efficiency. We notice a slight increase in Auger recombination, which leads to a decrease in the average life of the carriers at the surface, in addition to the formation of deposits and deformation on the surface

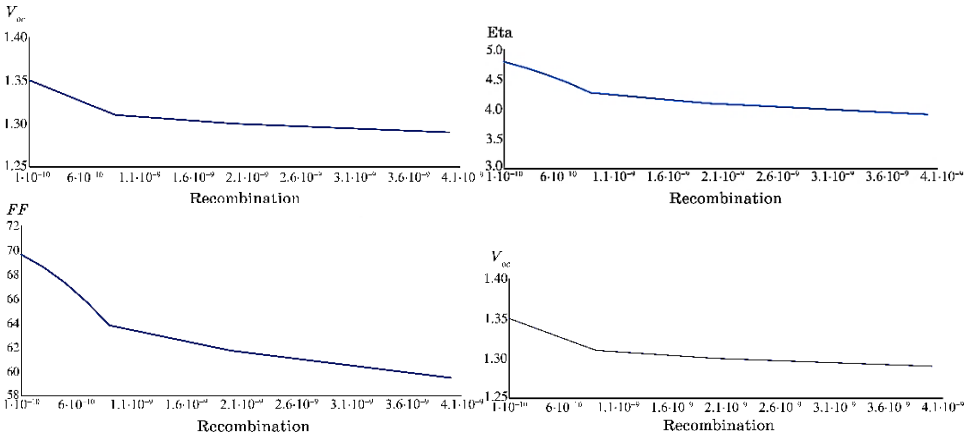

Fig. 11. Recombination as a function of cell output of the absorption layer.

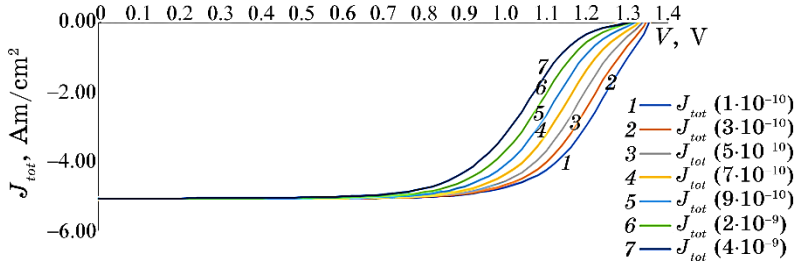

Fig. 12. Voltage as a function of current for different recombination values of the absorber layer.

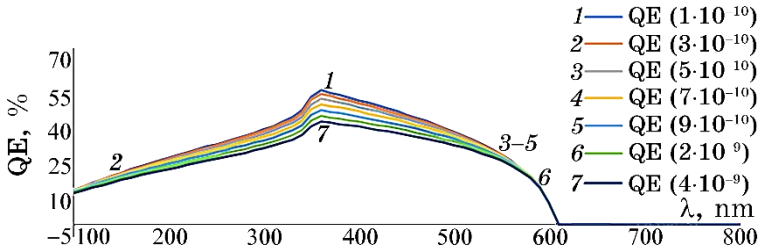

Fig. 13. Wavelength as a function of quantum efficiency for different recombination values of the absorption layer.

TABLE 4. Meaning of the symbols used in the research.

Mean of Symbol	Symbol	Mean of Symbol	Symbol
Open circuit voltage	V_{oc}	Electric filed	E
Conversion efficiency	η	charge	q
Maximum power	$P_{\max}$	Holes constriction	P
Actual power	P_t	Electron constriction	n
Input power	P_{in}	Acceptance consternation	N_A^-
Time of minority carriers	τ	Electron current density	J_n
Defects concentration	N_t	Holes current density	J_p
Heat velocity	V_{th}	Electron generation rate	G_n
Conductivity	σ	holes generation rate	G_p
Various concentrations of minority carriers	Δn	The rate of electron recombination	R_n
saturation current	I_0	The rate of holes recombination	R_p
The propagation length of electrons	L_e	Electron diffusion constant	D_n
The propagation length of holes	L_p	Holes diffusion constant	D_p
Electron concentration of pure semiconductor	n_i^2	Electron mobility	μ_n
Quantitative efficiency	QE	Holes mobility	μ_p
Spectral acceptance	R_λ	Fill factor	FF
Wave length	λ	Short circuit current	J_{sc}

[34]. Quantum efficiency is zero at long wavelength because no light can be absorbed below the forbidden energy gap.

5. CONCLUSIONS

The OMeATP/$Cs_2AgBiBr_6$/TiO_2/FTO cell was simulated using the SCAPS program and compared with an experimental cell. A very

large convergence was found between theoretical and experimental. The cell was also improved by increasing the work function. It was noted that increasing the distortion of the back reflection layer increases the performance of the cell to return photons to the cell. The thickness of the absorption layer has a significant impact on the performance of the cell. We noticed that increasing the thickness increases the efficiency of the cell due to increasing the absorption coefficient, and decreasing recombination increases the cell efficiency because recombination reduces the generation of the electron-gap pair.

REFERENCES

1. Zhenyang Liu, Hanjun Yang, Junyu Wang, Yucheng Yuan, Katie Hills-Kimball, Tong Cai, Ping Wang, Aiwei Tang, and Ou Chen, *Nano Letters*, **21**, Iss. 4: 1620 (2021); https://doi.org/10.1021/acs.nanolett.0c04148
2. Masataka Higashiwaki, Kohei Sasaki, Akito Kuramata, Takekazu Masui, and Shigenobu Yamakoshi, *phys. status solidi (a)*, **211**, No. 1: 21 (2014); https://doi.org/10.1002/pssa.201330197
3. Miao He, Qing Zeng, and Lijuan Ye, *Crystals*, **13**, No. 10: 1434 (2023); https://doi.org/10.3390/cryst13101434
4. Xing Chen, Kewei Liu, Zhenzhong Zhang, Chunrui Wang, Binghui Li, Haifeng Zhao, Dongxu Zhao, and Dezhen Shen, *ACS Appl. Mater. Inter.*, **8**, Iss. 6: 4185 (2016); https://doi.org/10.1021/acsami.5b11956
5. Sudheer Kumar, and R. Singh, *phys. status solidi (RRL)*, **7**, Iss. 10: 781 (2013); https://doi.org/10.1002/pssr.201307253
6. D. Y. Guo, Z. P. Wu, Y. H. An, P. G. Li, P. C. Wang, X. L. Chu, X. C. Guo, Y. S. Zhi, M. Lei, L. H. Li, and W. H. Tang, *Appl. Phys. Lett.*, **106**, No. 6: 042105 (2015); https://doi.org/10.1063/1.4907174
7. R. H. Al-Saqa, and I. K. Jassim, *Journal of Nanomaterials & Biostructures*, **18**, No. 1: 165 (2022); doi:10.15251/DJNB.2023.181.165
8. Rikiya Suzuki, Shinji Nakagomi, Yoshihiro Kokubun, Naoki Arai and Shigeo Ohira, *Appl. Phys. Lett.*, **94**, No. 22: 222102 (2009); https://doi.org/10.1063/1.3147197
9. K. Sasaki, M. Higashiwaki, A. Kuramata, T. Masui, and S. Yamakoshi, *IEEE Electron. Device Lett.*, **34**, No. 4: 493 (2013); https://doi.org10.1109/LED.2013.2244057
10. Masataka Higashiwaki, *AAPPS Bull.*, **32**: 3 (2022); https://doi.org/10.1007/s43673-021-00033-0
11. Kohei Sasaki, Masataka Higashiwaki, Akito Kuramata, Takekazu Masui, and Shigenobu Yamakoshi, *J. Cryst. Growth*, **378**: 591 (2013); https://doi.org/10.1016/j.jcrysgro.2013.02.015
12. O. M. Bordun, B. O. Bordun, I. Yo. Kukharskyy, and I. I. Medvid, *J. Appl. Spectrosc.*, **86**, No. 6: 1010 (2020); https://doi.org/10.1007/s10812-020-00932-4
13. Ashwin Kumar Saikumar, Shraddha Dhanraj Nehate, and Kalpathy B Sundaram, *ECS J. of Solid State Science and Technol.*, **8**, No. 7: Q3064 (2019); https://doi.org/10.1149/2.0141907jss
14. Lingyi Kong, Jin Ma, Caina Luan, Wei Mi, and Yu Lv, *Thin Solid Films*, **520**,

No. 13: 4270 (2012); https://doi.org/10.1016/j.tsf.2012.02.027
15. O. M. Bordun, B. O. Bordun, I. I. Medvid, and I. Yo. Kukharskyy, *Acta Physica Polonica A*, **133**, No. 4: 910 (2018); https://doi.org/10.12693/APhysPolA.133.910
16. K. H. Choi and H. C. Kang, *Materials Letters*, **123**: 160 (2014); https://doi.org/10.1016/j.matlet.2014.03.038
17. C. B. Willingham, J. M. Wahl, P. K. Hogan, L. C. Kupferberg, T. Y. Wong, and A. M. De, *Proc. SPIE*, **5078**: 179 (2003); https://doi.org/10.1117/12.500986
18. T. Igarashi, M. Ihara, T. Kusunoki, K. Ohno, T. Isobe, and M. Senna, *Appl. Phys. Lett.*, **76**, No. 12: 1549 (2000); https://doi.org/10.1063/1.1260921
19. O. M. Bordun, I. M. Bordun, and S. S. Novosad, *J. Appl. Spectr.*, **62**, No. 6: 1060 (1995); https://doi.org/10.1007/BF02606760
20. K. Wasa, M. Kitabatake, and H. Adachi, *Thin Film Materials Technology: Sputtering of Compound Materials* (New York: Springer–William Andrew Inc Publishing: 2004).
21. O. M. Bordun, B. O. Bordun, I. J. Kukharskyy, I. I. Medvid, O. Ya. Mylyo, M. V. Partyka, and D. S. Leonov, *Nanosistemi, Nanomateriali, Nanotehnologii*, **17**, Iss. 1: 123 (2019); https://doi.org/10.15407/nnn.17.01.123
22. Carl V. Thompson, *Sol. State Phys.*, **55**: 269 (2001); https://doi.org/10.1016/S0081-1947(01)80006-0
23. Carl V. Thompson, *J. Appl. Phys.*, **58**: 763 (1985); https://doi.org/10.1063/1.336194
24. O. M. Bordun, B. O. Bordun, I. Yo. Kukharskyy, I. I. Medvid, I. I. Polovynko, Zh. Ya. Tsapovska, and D. S. Leonov, *Nanosistemi, Nanomateriali, Nanotehnologii*, **19**, Iss. 1: 159 (2021); https://doi.org/10.15407/nnn.19.01.159
25. J. E. Palmer, C. V. Thompson, and Henry L. Smith, *J. Appl. Phys.*, **62**, No. 6: 2492 (1987); https://dx.doi.org/10.1063/1.339460
26. O. M. Bordun, I. O. Bordun, I. M. Kofliuk, I. Yo. Kukharskyy, I. I. Medvid, Zh. Ya. Tsapovska, and D. S. Leonov, *Nanosistemi, Nanomateriali, Nanotehnologii*, **20**, Iss. 1: 91 (2021); https://doi.org/10.15407/nnn.20.01.091
27. Tejaswini Sahoo and Paresh Kale, *Advanced Materials Interfaces*, **8**, Iss. 23: 2100649 (2021); https://doi.org/10.1002/admi.202100649
28. Sophie de Reguardati, Juri Pahapill, Alexander Mikhailov, Yuriy Stepanenko, and Aleksander Rebane, *Optics Express*, **24**, Iss. 8: 9053 (2016); https://doi.org/10.1364/OE.24.009053
29. Amrita Masurkar and Ioannis Kymissis, *Applied Physics Reviews*, **2**, Iss. 3: (2015); https://doi.org/10.1063/1.4926767
30. Mahmood M. Saleh, Hamadi Khemakhem, Ismel K. Jassim, and Read Hashim Al-Saqa, *Ochrona przed Korozją*, **67**, Nr. 1: 9 (2024); doi:10.15199/40.2024.1.2
31. Henry Kressel, *Semiconductors and Semimetals*, **16**: 1 (1981); https://doi.org/10.1016/S0080-8784(08)60128-3
32. Mehdi Leilaeioun and Zachary C. Holman, *Journal of Applied Physics*, **120**, Iss. 12: 123111 (2016); https://doi.org/10.1063/1.4962511
33. Raed Hashim Al-Saqa, Ismail Kalil Jassim, and Mohammad Mahmood Uonis, *Ochrona przed Korozją*, **66**, Nr. 8: 243 (2023); doi:10.15199/40.2023.8.3
34. Richard Haight, *Surface Science Reports*, **21**, Iss. 8: 275 (1995); https://doi.org/10.1016/0167-5729(95)00002-X